Journal of Computational Applied Mechanics 2022, 53(4): 571-584

DOI: 10.22059/jcamech.2022.348052.750

RESEARCH PAPER

Numerical Study on Convective Heat Transfer Characteristics of Single and Hybrid Nanofluids Flow Through Rectangular Conduits under Turbulent Flow with Uniform Heat Flux

Avik Ray [a], Sumanta Banejee [a], Prokash Chandra Roy [b,*]

[a] *Mechanical Engineering, Heritage Institute of Technology, Kolkata, India*
[b] *Mechanical Engineering, Jadavpur University, Kolkata, India*

Abstract

In this paper numerical analysis is carried out to find out the heat transfer performance of Al_2O_3/Cu nanofluid and Al_2O_3 nanofluid for different nanoparticle mixture ratios dispersed in water. The Al_2O_3 and Al_2O_3/Cu are simulated to flow in between a plain linear pipe with rectangular cross section. The channel is uniformly heated under constant wall heat flux conditions. The computational model is validated with experimental results from a recent literature study for Nusselt number within 7.89 % error and friction factor within 8.55% error. The simulation studies are performed with 0.5 %, 1.0% and 2.0% volume fraction of nano particle in the carrier fluid. The Reynolds number varies with the flow velocity, and ranges from 2000 to 12000 for the present study. The heat flux applied along the tube is ~$7955\ W/m^2$ and corresponds to realistic values obtained from literature review. The impacts of the flow Reynolds number, volume fraction and composition of nanofluids on heat transfer characteristics and friction factor are analysed for the hybrid nanofluid, and compared with the thermal performance of the chosen single-particle nanofluid. The validation of the numerical model has been performed with the published experimental results available in literature. The studies reveal that in comparison to water, the heat transfer coefficients of Al_2O_3 nanofluid are higher by 2.7%, 5.2%, and 10.9%, while those of Al_2O_3/Cu nanofluid are higher by 4.1%, 8.0%, and 16.2%, respectively, for (nanoparticle) volume fractions of 0.5%, 1.0%, and 2.0%. As compared to other working fluids, 2% Al_2O_3 shows the highest pressure drop. The thermal performance of the Al_2O_3/Cu hybrid nanofluid is better to the single-particle Al_2O_3 nanofluid dispersed in water. The study shows that for any representative value of volume fraction for the single-particle or hybrid nanofluid, the wall-averaged Nusselt number and the pressure drop increases monotonically with the Reynolds number.

Keywords: Forced convection; Heat transfer coefficient; Hybrid nanofluid; Single particle nanofluid; Volume fraction;

* Corresponding author.
E-mail address: avik.ray@heritageit.edu

1. Introduction and Background

To meet the ever-increasing demands of electronic devices, advanced cooling devices must be small and high-performing in order to ensure stable system operation. [1]. However, inherently low thermal conductivity delimits the development of energy-effective heat transfer fluids that are needed for ultra-efficient cooling applications. Due to this limitation on further improvements in the thermophysical properties of traditional fluids, the R &D trends have progressively shifted to nanofluids applications in heat transfer systems [2, 3].In Modern days, nanotechnology can create metallic or non-metallic particles $\sim \boldsymbol{nm}$ dimensions, having identical optical, mechanical, electrical, magnetic, and thermal behavior. These nanoparticles (with average sizes $\sim \mathbf{100}\ \boldsymbol{nm}$) may be suspended stably and dispersed uniformly in traditional heat transfer fluids like water, oil etc., by the use of suitable surfactants to prevent agglomeration. A good number of studies have found that effects of nanofluids on the heat transfer properties in thermal systems such as tubes.

A brief survey of technical literature is presented in this context. A computational model by Hussein et al. [4] has been developed to assess the heat transfer enhancement and friction factor for the flow of various types of nanofluids via tubes of three distinct forms (geometries), and have validated the same with experimental data available in literature. Water-based nanofluid comprising of TiO_2 nanoparticles with volume fractions 1%, 1.5%, 2% and 2.5% is used for three types (circular, elliptical and flat) of tubes. The results indicate heat transfer augmentation as the volume fraction increases. For this study, a CFD model based on FVM, has been used in FLUENT® environment. Experimental research on the forced convection heat transfer of TiO_2/water nanofluids flowing through channels with different cross sections has been done by Salimpour and D-Parizi [5]. According to the findings, nanofluids enhance the heat transfer in conduits. Moreover, experimental studies also revealed that, circular cross section conduit perform greater than square and triangular cross sections conduits in terms of a heat transfer performance. Hwang et al. [6] have calculated the heat transfer coefficient and pressure reduction of water-based Al_2O_3 nanofluids passing through a circular duct, considering homogeneous wall heat flux under the laminar flow regime. As compared with water, the heat transfer enhancement is observed to be $\sim 8\%$ at a volume fraction of $\sim 0.3\ vol\%$. In contrast to the rise in thermal conductivity, the improvement in convective heat transfer coefficient outnumbers from a wide margin. Based on scale analysis and numerical simulations, the study describes how rapid changes in bulk properties like nanoparticle concentration, thermal conductivity, and viscosity may have caused a flattening of velocity profiles. The result is a significant increase in heat transfer coefficient. In the experimental study conducted by Heris et al. [7], flow of two different grades of single-particle nanofluid continuum through circular tubes have been investigated. The tubes are subjected to constant wall-temperature boundary conditions. The nanofluid medium comprises of CuO and Al_2O_3 nanoparticles in water at various volume concentrations. The experiments emphasize that the popular Homogeneous Model (single-phase correlation with nanofluids properties) is insufficient to calculate heat transfer improvement of nanofluids. The studies reveal that both nanofluid-systems result in Nusselt number enhancements with increasing nanoparticle volume fraction and the Peclet number. However, at higher values of volume fraction, the $Al_2O_3/water$ system has higher heat transfer enhancement than the $CuO/water$ system.

Ghachem et al. [8] provides a 3-D Numerical analysis of CNT-Al_2O_3-Water hybrid nanofluid improved heat transfer inside a wavy-channeled cross-flow micro heat exchanger. The finite element approach was used to do this numerical analysis with regard to several factors such as flow speed, wave number, and nanoparticle concentration. Almeshaal et al. [9] have performed 3-D computational analysis on natural convection in a T-shaped enclosure, which is filled with $CNT - Al_2O_3$ hybrid nanofluid by stream function and vorticity method. The parameters are taken as enclosure dimension, volume percentage of nanoparticles, fraction of CNT presents, and the Rayleigh number. Mehryan et al. [9] presents a numerical model on natural convection heat transfer inside a T-shaped cavity filled with magnetic hybrid nanofluid, heated from the lower end and cooled from the upper chamber walls, with two different porous layers forming the cavity. Wide-ranging governing parameters have been carried out to study the flow development and heat transfer of hybrid nanofluid within the enclosure. Aminian et al. [10] presents a numerical model on the magnetic effects of $Al_2O_3 - CuO$ −water nanofluid filled inside a partitioned cylinder within a porous medium under laminar regime, where the cylinder walls are exposed to a continuous heat flux. The computations were done for a wide variety of governing factors. The effects of the Darcy number, Hartmann number, and magnetic field on heat transmission and pressure drop were studied. The goal of this research is to compare heat transfer coefficients, Nusselt number, pressure drop, and friction factor as important heat transfer parameters for internal forced convection of water, Al_2O_3 and Al_2O_3/Cunanofluids through a plain, straight rectangular duct under symmetrical and uniform heat flux. The comparison is performed for different Reynolds numbers, volume fractions and compositions of nanoparticles. One of the principal objectives of this work is to analyze heat transfer characteristics of a hybrid nanofluid synthesized by combining two nanoparticles in varied proportions, one with better stability and lower

thermal conductivity (Al_2O_3) and the other one with lesser stability and higher thermal conductivity (Cu). The results of this study could provide insights on the optimal mixing proportions of these nanoparticles in the (hybrid) nanofluid system, so as to achieve an effective balance between heat transfer enhancement on one hand, and rise in pressure drop on the other.

The foregoing literature review presents a brief survey of analytical, experimental and/or simulation studies largely devoted to flow and heat transfer characteristics of single particle nanofluid systems. However, research literature based on heat transfer studies using hybrid nanofluid as working medium are relatively less in the field of rectangular pipe used in solar collector, heat exchanger etc. The current study compares heat transfer coefficient, Nusselt number, pressure drop, friction factor, as heat transfer characteristics for water, Al_2O_3, and Al_2O_3/Cu nanofluids in a straight tube. The investigation is performed on different values of the Reynolds number as well as volume fraction of single and hybrid nanofluid. The novelty of the current study is to summarize the impact on heat transmission properties of hybrid nanofluid by combining two nanoparticles, Al_2O_3 (higher stability and lower thermal conductivity) and other Cu (lower stability and higher thermal conductivity) for different volume fractions of nanoparticles.

2. Nomenclature

C	Specific heat capacity $[J/kgK]$	V	Volume $[m^3]$	bf	Base fluid
D	Hydraulic Diameter $[m]$	ρ	Density $[kg/m^3]$	hnf	Hybrid nanofluid
$\bar{f}$	Friction factor	μ	Viscosity $[Pa.s]$	$np1$	Nano particle 1
h	Convective heat transfer coefficient $[W/m^2K]$	φ	Volume fraction	$np2$	Nano particle 2
k	Thermal conductivity $[W/mK]$	***Subscript***			
Nu	Nusselt number	np	Nano particle		
P	Pressure $[N/m^2]$	nf	Nanofluid		

3. Thermophysical Properties Measurements

Table 1 show the properties of the base fluid (water) and considered nanoparticles (Al_2O_3, Cu). The nano particles have a spherical form with $\sim 100\, nm$ size. Using the equations described in subsections 2.1 and 2.2, the thermophysical characteristics of single particle nanofluid and hybrid nanofluid systems are estimated. These equations are based on widely used models in the reviewed literature. The properties of Al_2O_3 are specified for a reference temperature of $300K$ (refer to Nomenclature list) [11, 12]. All of these properties have been modeled as temperature-independent [13].

Table 1. Properties of water and various nanoparticles

Property	Water	Al_2O_3	Cu
ρ	998.2	3970	8300
C	4182	765	420
k	0.6	40	401
μ	0.001	-	-

3.1 Single particle nanofluid properties

To estimate the thermophysical properties of single particle and hybrid nanofluids, widely-used models in the open literature are employed [14, 15]. The volume fraction of nanoparticles in nanofluid is expressed as [14, 16]:

$$\emptyset = \frac{V_{np}}{V_{bf}+V_{np}} \quad (1)$$

Eq. (1) relates the volume fraction of nanoparticles in nanofluid, volume of base fluid, and the volume of nanoparticles $\left(V_{np} = m_{np}/\rho_{np}\right)$. m_{np} is the nano particle mass.

The density of nanofluid is computed in terms of the volume fraction of nanoparticles, density of nanoparticles, and density of base fluid:

$$\rho_{nf} = (1-\phi)\rho_{bf} + \phi\rho_{np} \quad (2)$$

The specific heat of nanofluid can be described in terms of the specific heat of base fluid and the specific heat of nanoparticles:

$$C_{P_{nf}} = \frac{(1-\phi)\rho_{bf}C_{p,bf}+\phi\rho_{np}\,C_{p,np}}{\rho_{nf}} \quad (3)$$

The effective thermal conductivity of the nanofluid is specified in terms of the thermal conductivity of base fluid and thermal conductivity of nanoparticle:

$$k_{nf} = k_{bf}\left[\frac{(k_{np}+2k_{bf})-2\phi(k_{bf}-k_{np})}{(k_{np}+2k_{bf})+\phi(k_{bf}-k_{np})}\right] \quad (4)$$

The effective dynamic viscosity of the nanofluid can be expressed as a function of viscosity of base fluid the volume fraction of nanoparticles:

$$\mu_{nf} = \frac{\mu_{bf}}{(1-\phi)^{2.5}} \quad (5)$$

3.2 Hybrid nanofluid properties

The volume fraction of the hybrid nanofluid is expressed as the sum of the volume fractions of the respective components [8, 15]:

$$\emptyset_{hnf} = \emptyset_{np1} + \emptyset_{np2} \quad (6)$$

Once $\emptyset_{hnf}$ is calculated from Eq. (6), the density of the hybrid nanofluid can be evaluated from the volume fraction and density values of constituent nanoparticles and the base fluid density:

$$\rho_{nf} = \emptyset_{np1}\rho_{np1} + \emptyset_{np2}\,\rho_{np2} + (1 - \emptyset_{hnf})\rho_{bf} \quad (7)$$

The specific heat of hybrid nanofluid can be expressed in terms of the specific heats of nanoparticles 1 and 2, and the specific heat of the base fluid:

$$C_{p,hnf} = \frac{\emptyset_{np1}\rho_{np1}C_{p,np1}+\emptyset_{np2}\rho_{np2}C_{p,np2}+(1-\emptyset_{hnf})\rho_{bf}C_{p,bf}}{\rho_{hnf}} \quad (8)$$

The effective thermal conductivity of the hybrid nanofluid can now be calculated, in terms of the volume fractions and thermal conductivities of the constituent nanoparticles and the hybrid nanofluid:

$$k_{hnf} = \frac{\frac{\emptyset_{np1}k_{np1}+\emptyset_{np2}k_{np2}}{\emptyset_{hnf}}+2k_{bf}+2(\emptyset_{np1}k_{np1}+\emptyset_{np2}k_{np2})-2\emptyset_{hnf}k_{bf}}{\frac{\emptyset_{np1}k_{np1}+\emptyset_{np2}k_{np2}}{\emptyset_{hnf}}2k_{bf}-2(\emptyset_{np1}k_{np1}+\emptyset_{np2}k_{np2})+\emptyset_{hnf}k_{bf}} \quad (9)$$

Lastly, the effective viscosity of hybrid nanofluid is computed in terms of the viscosity of the base fluid, as well as the volume fractions of nanoparticles 1 and 2:

$$\mu_{hnf} = \mu_{bf}\,\frac{1}{(1-\emptyset_{np1}-\emptyset_{np2})^{2.5}} \quad (10)$$

4. Problem Description & Mathematical Model

The 3D computational region of the physical system is depicted in Fig. 1. The annular channel, made of copper, has a length is $1500\ mm$. The inner square has sides of $16\ mm$, and the outer square has side measuring $19\ mm$.. Considering constant wall heat-flux conditions, a copper conduit using water, single-particle, and hybrid nanofluids as working substance is explored using computational fluid dynamics (CFD) techniques [17-58]. The main objective of this study is to find out the fluid flow and heat transfer charecteristics in the channel. The uniform heat flux is symmetrically distributed on the surface of the tube [16]. The physical properties of copper considered for simulations are: $\rho_{Cu} = 8940\ kg/m^3$; $C_{p,Cu} = 376.8\ J/kgK$; $k_{p,Cu} = 401\ W/mK$ [16]. The heat flux input to the system is chosen in line with the experimental set up reported in [16]. In this study, a voltage regulator is installed in the test area, which supplies input power to the heater at a steady rate of $600\ W$. Keeping the same heat input rate, the (calculated) value of heat flux for the present configuration is $\approx 7955\ W/m^2$.

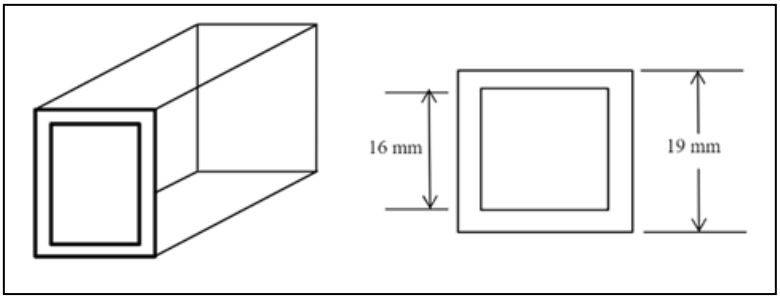

Fig. 1: Configuration of 3D channel

Considering flow of various working fluids, the conservation equations of mass, momentum and energy are solved

for the chosen channel configuration to simulate thermal and flow characteristics [59, 60].

Continuity Equation:

$$\nabla.\left(\rho\vec{V}\right) = 0 \tag{11}$$

Momentum Equation:

$$\nabla.\left(\rho\vec{V}\vec{V}\right) = -\nabla P + \nabla\cdot\tilde{\boldsymbol{\tau}} \tag{12}$$

Energy Equation:

$$\nabla\cdot\left(\rho\vec{V}h\right) = \nabla\cdot(k\nabla T) + \tilde{\boldsymbol{\tau}}:\nabla\vec{V} \tag{13}$$

The stress tensor $\tilde{\boldsymbol{\tau}}$ (Eq. (12) and Eq. (13)) is expressed in terms of velocity field $\vec{V}$ ($\tilde{\boldsymbol{\delta}}$ is the Kronecker delta):

$$\tilde{\boldsymbol{\tau}} = \mu\left[\nabla\vec{V} + \left(\nabla\vec{V}\right)^{T} - \frac{2}{3}\tilde{\boldsymbol{\delta}}\left(\nabla.\vec{V}\right)\right] \tag{14}$$

In Eqs. (11)-(14) P is the pressure field and h the specific enthalpy. The $k-\epsilon$ turbulence model has also been incorporated in the numerical analysis in line with [14]. Here k & ϵ are turbulent kinetic energy and turbulent dissipation rate.

The channel under continuous heat flux condition is simulated in the ANSYS® software environment to examine the flow and heat transfer characteristics of water and nanofluids. The simulations are carried out using a solution based on the Finite Volume Method. The Semi-Implicit Method for Pressure Linked Equations (SIMPLE) algorithm is adopted for the solution of the conservation equations, and the Power Law scheme is adopted for the discretization of convection-diffusion terms [61]. As already mentioned, the $k-\epsilon$ model for turbulent viscosity has been used. Detailed information on the methodology implemented for numerical analysis in ANSYS® has been reviewed for implementation [62]. The convergence criteria for all the field equations have been set at $\sim 10^{-8}$.

The boundary conditions are uniform heat flux ($\approx 7955\ W/m^2$) applied to walls of the channel with symmetrical distribution [18]. The inlet velocity, with different values of the Reynolds number for working fluids, and the pressure outlet conditions are provided. The Reynolds number has been varied from ≈ 2000 to ≈ 12000, and the inlet fluid temperature is ≈ 298.15 K. The working fluids considered are water, single-particle Al_2O_3- nanofluid and hybrid $Al_2O_3/Cu-$ nanofluid. The thermal properties of the base fluid and the related nanoparticles are used to evaluate the thermophysical properties of single-particle and hybrid nanofluids. In the numerical analysis, three volume fractions of 0.5%, 1% and 2% are used. Both nanoparticle compositions are combined in equal amounts in hybrid nanofluids. When solving equations with the specified boundary conditions, it is presumed that the flow is uniform, stable, and incompressible [15]. The analysis takes into account the laminar and conventional $k-\varepsilon$ turbulence models.

5. Evaluation of Heat Transfer and Fluid Flow Parameters

The average heat transfer coefficient $\left(=\bar{h}\right)$ is calculated considering the heat transfer rate $\left(=\dot{Q}\right)$, the heat transfer area $(=A)$, the average surface temperature of the wall $(=T_s)$ and the bulk mean temperature of fluid $(=T_b)$: [14, 63]

$$\bar{h} = \dot{Q}/A(T_s - T_b) \tag{15}$$

Given the rate of mass flow $\left(=\dot{m}_f\right)$ of fluid and the computed values of the fluid mean temperatures at the inlet $\left(=T_{b,i}\right)$ and the exit $\left(=T_{b,o}\right)$ sections, the heat transfer rate $\left(=\dot{Q}\right)$ by the working fluid is evaluated as:

$$\dot{Q} = \dot{m}_f c_p\left(T_{b,o} - T_{b,i}\right) \tag{16}$$

The average Nusselt number $(=\overline{Nu})$ is calculated considering the hydraulic diameter $(=D)$ of rectangular channel:

$$\overline{Nu} = \bar{h}D/k_f \tag{17}$$

The average friction factor $(\bar{f})$ is determined by the pressure drop $(=\Delta P)$, length of the channel $(=L)$, hydraulic diameter, fluid density and the average velocity $(=\bar{U})$:

$$\bar{f} = \frac{\Delta P}{\left(\frac{L}{D}\right)\left(\frac{\rho U^2}{2}\right)} \tag{18}$$

In Eq. (18), the pressure drop is expressed as the difference of the inlet and outlet fluid pressures:

$$\Delta P = P_{f,i} - P_{f,o} \tag{19}$$

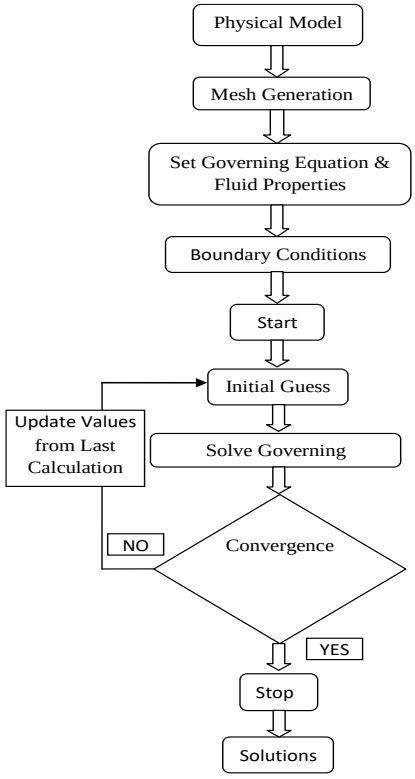

Fig 1(a): Flow chart of numerical procedure

5.1 Grid independence test

Grid independence has been performed in ANSYS® platform in order to obtain the appropriate size of mesh (consequently, optimum number of mesh elements). In this study, tetrahedral meshing is considered. Grid independence has been verified by five different numbers of mesh elements, ranging from 10^5 to $7X10^5$. Fig. 2 (a) and Fig. 2 (b) depict the variations of the Nusselt number and the friction factor, as the number of grid elements is increased. The variation trends show that the marginal change in the Nusselt number and the friction factor are in between $\pm 2\%$ over the grid item quantity of 555291. Beyond this grid component number, the amount of elements used for computations has almost no effect on the simulation outcomes. For this reason a total of 555291 mesh elements is selected for the present study, as a trade-off between increased accuracy and increased computational costs.

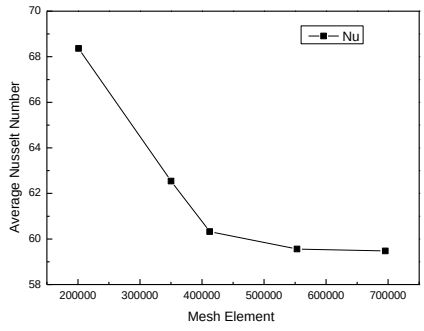

Fig. 2(a): Variation of average Nusselt number with number of elements

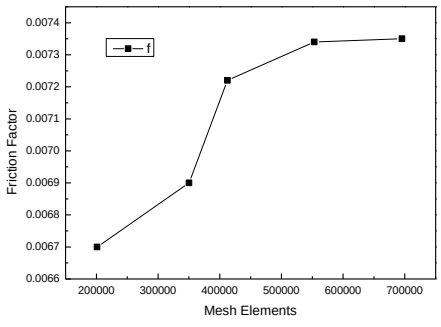

Fig. 2(b): Variation of friction factor with mesh elements number

6. Results and Discussion

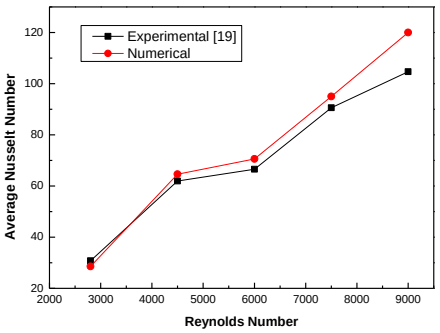

Fig. 3(a): Variation of average Nusselt number with Reynolds number

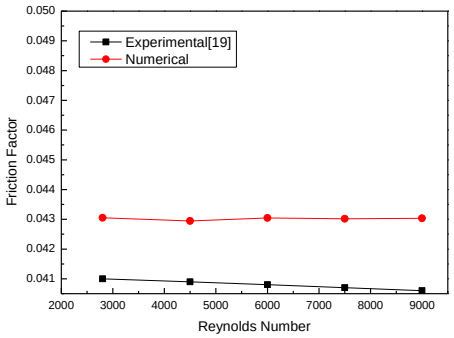

Fig. 3(b): Variation of friction factor with Reynolds number

6.1. Validation

The validation of the numerical model based on CFD techniques has been conducted with the experimental results presented in [16] for circular tube configuration, for the same set of temperature and pressure boundary conditions. From the perspective of heat transfer study, the experimentally-evaluated and the numerically-calculated values of the average Nusselt number (Fig. 3(a)) and the friction factor (Fig. 3(b)) has been compared considering varying values of the Reynolds number. For all Reynolds number variations investigated, the average variance between experimental and numerical values of Nusselt number is 7.89% and that of friction factor is 8.55%.

6.2. Properties of Nanofluid

The calculated values of nanofluid thermophysical properties (putting $\emptyset_{hnf} = 0.02;\ \emptyset_{np1} = 0.01;\ \emptyset_{np2} = 0.01$ in Eq. (6) – Eq. (10)) are listed in Table 2. For the hybrid Al_2O_3/Cu nanofluid, the nanoparticles are mixed in the same proportion (i.e. $50/50$ %).

Table 2: Properties of Nanofluids [as calculated by Eq. (6) – Eq. (10)]

Nanofluid	Density (kg/m^3)	Specific Heat (J/kgK)	Thermal Conductivity (W/mK)	Viscosity $(Pa.s)$
0.5% Al_2O_3	1013.059	4115.047	0.6086	0.001013
0.5% Al_2O_3/Cu	1023.884	4072.637	0.612	0.001013
1% Al_2O_3	1027.918	4050.029	0.617	0.001025
1% Al_2O_3/Cu	1049.568	3968.626	0.624	0.001025
2% Al_2O_3	1057.636	3925.475	0.635	0.001052
2% Al_2O_3/Cu	1100.936	3775.164	0.649	0.001052

6.3. Comparing the Heat Transfer Characteristics

In the current section analyzes the heat transfer characteristics, which includes the thermal qualities of heat transfer coefficient and, consequently, the Nusselt number. The flow properties of pressure drop and friction factor are also discussed for the chosen Al_2O_3 and Al_2O_3/Cu nanofluid systems.

6.3.1 Heat Transfer Coefficient

Figure 4(a) displays the heat transfer enhancement dependents on Reynolds number, considering various term of the nanoparticles volume percentage of in either of the chosen systems. It can be observed that the heat transfer

coefficients among all functioning liquids rise monotonically with the increments of Reynolds number [20] and the volume fraction of the nanoparticles. Additionally, given the same volume fraction, the heat transfer coefficient measured for the hybrid nanofluid is superior to the single-particle nanofluid. It is a result to the inclusion of Cu nanoparticles having better thermal conductivity in the former nanofluid grade. The heat transfer coefficients of Al_2O_3 nanofluid are respectively higher by $\approx 2.7\%$, $\approx 5.2\%$ and $\approx 10.9\%$, and those of Al_2O_3/Cu nanofluid are respectively higher by $\approx 4.1\%$, $\approx 8.0\%$ and $\approx 16.2\%$, for (nanoparticle) volume fractions of 0.5%, 1.0% and 2.0%, in contrast with water. The study reveals that Al_2O_3/Cu nanofluid with 2.0% volume fraction indicates the greatest value of heat transfer coefficient across all the selected grades of working fluids. Once the Reynolds number rises from 2000 to 12000, it is observed that the heat transfer coefficient for Al_2O_3/Cu nanofluids with 2.0% volume fraction increases by ≈ 5.891 times.

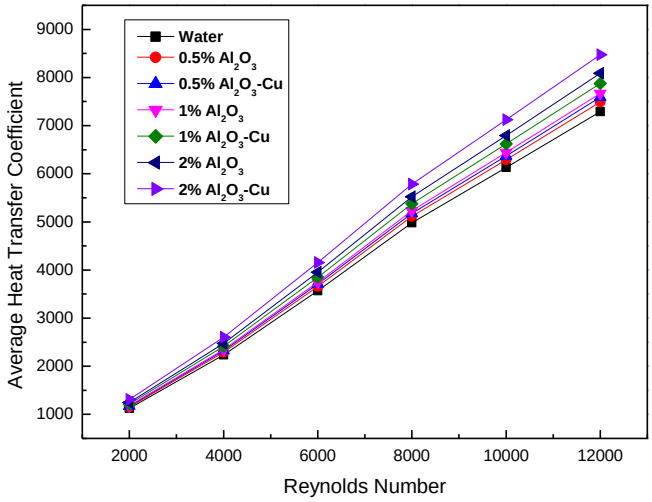

Fig. 4(a): Plots of average heat transfer coefficient versus the flow Reynolds number

6.3.2 Nusselt Number

Figure 4(a) illustrates that the Nusselt number changes as the Reynolds number rises for various working fluids (b). The Nusselt number is the dimensionless analogue of the heat transfer coefficient. The Nusselt number rises as the volume concentration and turbulence level rise. The hybrid-grade Al_2O_3/Cu nanofluid presents a better performance in heat transfer enhancement, as compared to Al_2O_3 nanofluid due to its higher thermal conductivity. It can be concluded that, in the presence of solid nanoparticles in water (base fluid) has improved thermal conductivity, which becomes better when more nanoparticles are spread throughout the medium. This results in monotonic rise in heat transfer coefficient as the volume percentage of nanoparticles rises. The average Nusselt numbers ($= \overline{Nu}$) evaluated in this study are listed as follows: $\overline{Nu} \approx 207.71$ for the base fluid (water); $\overline{Nu} \approx 210.3; 212.36; 217.62$ respectively for $0.5\%; 1\%; 2\%$ Al_2O_3 single-particle nanofluid; and $\overline{Nu} \approx 211.97; 215.59; 222.92$ for $0.5\%; 1\%; 2\%$ Al_2O_3/Cu hybrid nanofluid, all measured at Reynolds number ≈ 12000. The 2% Al_2O_3/Cu nanofluid exhibited better Nusselt number value across all Reynolds number in contrast with other working fluids. The wall-averaged Nusselt number of 2% Al_2O_3/Cu nanofluid increases from $\overline{Nu} \approx 74$ to $\overline{Nu} \approx 222.92$ as the chosen range of Reynolds number.

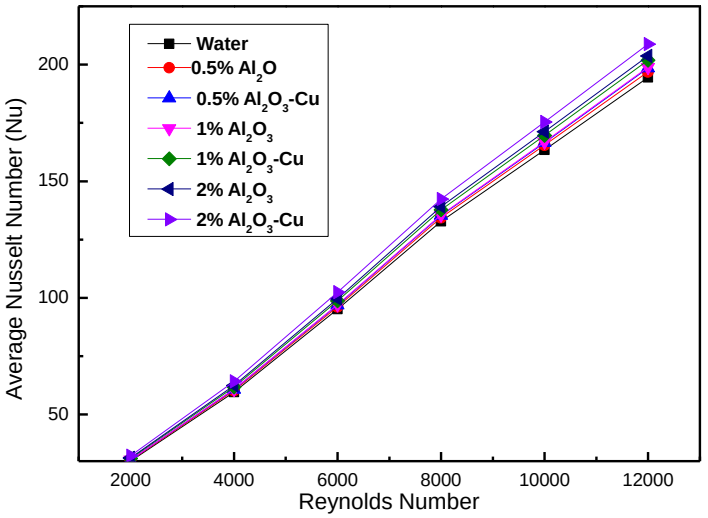

Fig. 4(b): Plots of average wall Nusselt number versus the flow Reynolds number

6.3.3 Pressure Drop

The Fig.5 (a) shows the change in the pressure reduction of water, Al_2O_3 and $Al_2O_3/Cu$with different volume percentage and Reynolds number. For all working fluids, As the Reynolds number rises, the pressure drop grows owing to rise in the turbulence intensity. Furthermore, the trend of variation of pressure drop with Reynolds number varies amongst the working fluids, which highlights the novelty of the present work. The exponential variation trend, as found in the present study, is confirmed by published open literature [64]. Figure 5(a) shows that the pressure drop rises monotonically with increasing values of the Reynolds number. This is expected, as the rise in Reynolds number is associated with the rise in (mean) flow velocity that causes enhanced values of the average wall shear stress. The pressure drop for single-particle and hybrid nanofluids are superior to water, owing to higher values of effective viscosity coefficients. In addition, the viscosity values of Al_2O_3 and Al_2O_3/Cu raises at higher percentage nanoparticles because of larger quantities of nanoparticles are dispersed into the water. This contributes to higher pressure drop with greater volume fraction for Al_2O_3 and Al_2O_3/Cu. For the chosen set of flow conditions, $2\%\ Al_2O_3$ shows the highest pressure drop compared to others working fluids. As calculations show, the pressure drops of $2\%\ Al_2O_3$ nanofluid and $2\%\ Al_2O_3/Cu$ nanofluid are higher by $\approx 4.7\%$ and $\approx 0.61\%$ respectively. Furthermore up to 6000 Re number pressure drop is not creates any problem as volume fractions is increases. At higher Re number pressure drop raises significantly as volume fractions increases. As a result of that higher pumping power is required to flow the fluid.

6.3.4 Friction factor

The effect of different values of the volume concentration (of nanoparticles) on friction factor is shown in Fig. 5(b), in the selected range of $0.5\% - 2\%$ particle concentrate on. The results show that, for any value of (disperse particle) concentration, the friction factor decreases with rise in the Reynolds number [59, 63].

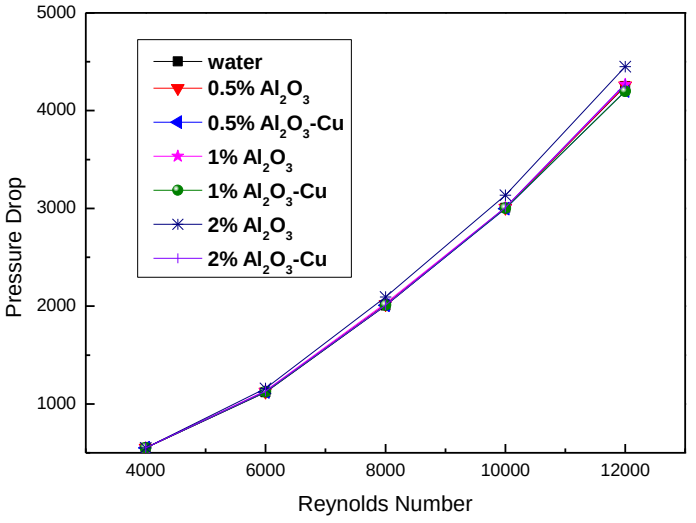

Fig 5(a): Variations of pressure drop for water, single-particle and hybrid nanofluid systems with the Reynolds number

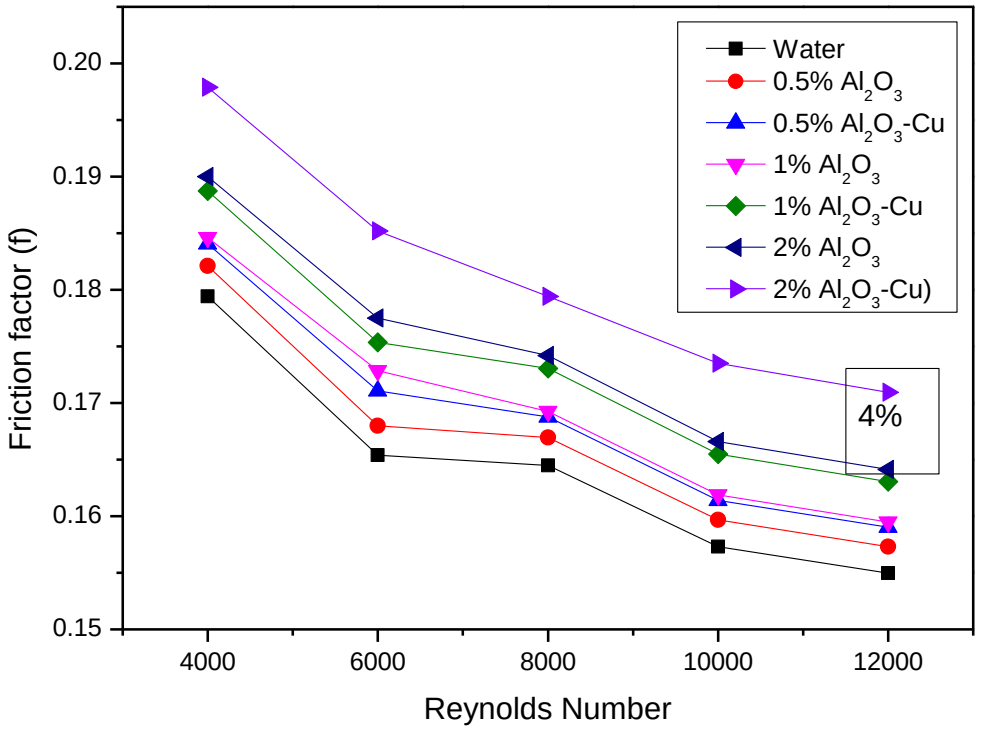

Fig 5(b): Variations of friction factor for water, single-particle and hybrid nanofluid systems with Reynolds number

We observe that $\bar{f} = \frac{\Delta P}{\left(\frac{L}{D}\right)\left(\frac{\rho \bar{U}^2}{2}\right)} \equiv \frac{\Delta P}{\frac{1}{2}Re_L^2\left(\frac{\mu^2}{\rho L D}\right)} \sim \frac{\Delta P}{\frac{1}{2}Re_L^2}$ $\left(Re_L = \frac{\rho \bar{U} L}{\mu}\right)$; this implies that the average friction factor varies directly as the pressure drop and inversely as the square of the Reynolds number $(= Re_L)$. As the Reynolds number increase, the rate at which $\bar{f}$ decreases outweighs the rate of $\bar{f}$ rise with pressure drop (that happens for increasing values of the Reynolds number). The net effect is that $\bar{f}$ decreases monotonically with increasing values of Re_L However, for any given value of the Reynolds number, single and hybrid nanofluid shows higher the friction factor

than water. This is because of the higher viscosity of nanofluid in contrast with water. Since hybrid nano fluid have a higher density compared to single particle nano fluid, effectively it leads to a lower velocity of hybrid nanofluid compared to single particle nanofluid. Therefore despite of lower pressure drop hybrid nanofluid shows a higher friction coefficient than single particle nanofluid. While comparing the wall-averaged friction factor values for hybrid and single particle nanofluids at 2% volume fraction, a greater rise of $\bar{f}$ ($\approx 4\%$) is observed. Although hybrid nanofluid with 2% volume fraction will enhance heat transfer rate (as compared to single particle nanofluid with 2% volume fraction) this comes adverse effect of increases friction loss. This is undesirable. This is due to lower energy density $\left(\frac{\rho \bar{U}^2}{2}\right)$ obtained of hybrid nanofluid for a particular volume fraction. At $Re_L \approx 12000$ the energy density of 2% hybrid Al_2O_3/Cu and single-particle Al_2O_3 are respectively evaluated as $\approx 282.7\ J/m^3$ and $\approx 294.3\ J/m^3$ respectively. As the value of $\bar{f}$ varies inversely with the energy density, one can observe that the friction factor for the hybrid grade increases significantly over its single-particle counterpart. This, in turn, implies higher frictional loss. However, at 0.5% and 1% volume fractions, the friction factor increases by about $\approx 1\%$ and $\approx 2.3\%$, respectively. The system is found to be cooled by hybrid nanofluid at low volume fractions without noticeable increase in frictional loss.

7. Conclusion

In this study, a CFD analysis has been conducted in ANSYS®/FLUENT® environment to investigate, respectively, the effects of single-particle $Al_2O_3 -$ nanofluid flow and hybrid $Al_2O_3/Cu -$ nanofluid flow on heat transfer and pressure drop inside a rectangular tube. For the numerical analysis, 555291 number of mesh is considered throughout the computational domain, corresponding to a size of 2 mm. On the fluid domain, inflation layers are used to account for the effect of boundary layers. Numerical and experimental data published in the research paper have satisfactorily validated the CFD study [16]. The study shows that,

(a) For single and hybrid nanofluids, the values of the average heat transfer coefficient (and, hence, the average Nusselt number) rise with the increase in Reynolds number and volume fraction of nanoparticles. 2.0 % Al_2O_3 and 2.0 % Al_2O_3/Cu nanofluids have higher heat transfer coefficients than water by $\approx 10\%$ and $\approx 16\%$ respectively.

(b) However, pressure drop and friction factor also improved against volume fraction, indicating larger requirement of pumping power to maintain flow. However, pressure drop exhibit growing trend and friction factor decreases by increasing Reynolds number. 2.0 % Al_2O_3 nanofluid and 2.0 % Al_2O_3/Cu nanofluid have higher pressure drops than water by $\approx 4.7\%$ and $\approx 0.61\%$ respectively.

(c) Although hybrid nanofluid with 2% volume fraction will enhance heat transfer rate (as compared to single particle nanofluid with 2% volume fraction) this comes adverse effect of increases friction loss. This is undesirable.

Reference

[1] M. Dadhich, O. S. Prajapati, V. Sharma, Investigation of boiling heat transfer of titania nanofluid flowing through horizontal tube and optimization of results utilizing the desirability function approach, *Powder Technology*, Vol. 378, pp. 104-123, 2021.

[2] N. A. Sheikh, D. L. Chuan Ching, I. Khan, A comprehensive review on theoretical aspects of nanofluids: Exact solutions and analysis, *Symmetry*, Vol. 12, No. 5, pp. 725, 2020.

[3] M. B. Kim, H. G. Park, C. Y. Park, Change of thermal conductivity and cooling performance for water based Al2O3-surfactant nanofluid with time lapse, *International Journal of Air-Conditioning and Refrigeration*, Vol. 26, No. 01, pp. 1850009, 2018.

[4] A. M. Hussein, K. Sharma, R. Bakar, K. Kadirgama, The effect of cross sectional area of tube on friction factor and heat transfer nanofluid turbulent flow, *International Communications in Heat and Mass Transfer*, Vol. 47, pp. 49-55, 2013.

[5] M. R. Salimpour, A. Dehshiri-Parizi, Convective heat transfer of nanofluid flow through conduits with different cross-sectional shapes, *Journal of Mechanical Science and Technology*, Vol. 29, No. 2, pp. 707-713, 2015.

[6] K. S. Hwang, S. P. Jang, S. U. Choi, Flow and convective heat transfer characteristics of water-based Al2O3 nanofluids in fully developed laminar flow regime, *International journal of heat and mass transfer*, Vol. 52, No. 1-2, pp. 193-199, 2009.

[7] S. Z. Heris, S. G. Etemad, M. N. Esfahany, Experimental investigation of oxide nanofluids laminar flow convective heat transfer, *International communications in heat and mass transfer,* Vol. 33, No. 4, pp. 529-535, 2006.

[8] K. Ghachem, W. Aich, L. Kolsi, Computational analysis of hybrid nanofluid enhanced heat transfer in cross flow micro heat exchanger with rectangular wavy channels, *Case Studies in Thermal Engineering,* Vol. 24, pp. 100822, 2021.

[9] M. A. Almeshaal, K. Kalidasan, F. Askri, R. Velkennedy, A. S. Alsagri, L. Kolsi, Three-dimensional analysis on natural convection inside a T-shaped cavity with water-based CNT–aluminum oxide hybrid nanofluid, *Journal of Thermal Analysis and Calorimetry,* Vol. 139, No. 3, pp. 2089-2098, 2020.

[10] E. Aminian, H. Moghadasi, H. Saffari, Magnetic field effects on forced convection flow of a hybrid nanofluid in a cylinder filled with porous media: A numerical study, *Journal of Thermal Analysis and Calorimetry,* Vol. 141, No. 5, pp. 2019-2031, 2020.

[11] W. Arear, A. Zeiny, M. A. S. Al-Baghdadi, Influence of Al2O3-Water Nanofluid Coolant on Thermal Performance of Hydrogen PEM Fuel Cell Stacks, in *Proceeding of,* IOP Publishing, pp. 012064.

[12] B. Devakki, S. Thomas, Experimental investigation on absorption performance of nanofluids for CO2 capture, *International Journal of Air-Conditioning and Refrigeration,* Vol. 28, No. 02, pp. 2050017, 2020.

[13] S. R. Chaurasia, R. Sarviya, Comparative thermal performance analysis with entropy generation on helical screw insert in tube with number of strips with nanofluid at laminar flow regime, *International Communications in Heat and Mass Transfer,* Vol. 122, pp. 105138, 2021.

[14] K. S. Garud, M.-Y. Lee, Numerical Investigations on Heat Transfer Characteristics of Single Particle and Hybrid Nanofluids in Uniformly Heated Tube, *Symmetry,* Vol. 13, No. 5, pp. 876, 2021.

[15] M. Sanches, G. Marseglia, A. Ribeiro, A. Moreira, A. Moita, Nanofluids Characterization for Spray Cooling Applications. Symmetry 2021, 13, 788, s Note: MDPI stays neu-tral with regard to jurisdictional claims in …, 2021.

[16] M.-Y. Lee, J.-H. Seo, H.-S. Lee, K. S. Garud, Power generation, efficiency and thermal stress of thermoelectric module with leg geometry, material, segmentation and two-stage arrangement, *Symmetry,* Vol. 12, No. 5, pp. 786, 2020.

[17] M. Mohammadi, A. Farajpour, A. Moradi, M. Hosseini, Vibration analysis of the rotating multilayer piezoelectric Timoshenko nanobeam, *Engineering Analysis with Boundary Elements,* Vol. 145, pp. 117-131, 2022.

[18] M. Mohammadi, A. Rastgoo, Primary and secondary resonance analysis of FG/lipid nanoplate with considering porosity distribution based on a nonlinear elastic medium, *Mechanics of Advanced Materials and Structures,* Vol. 27, No. 20, pp. 1709-1730, 2020.

[19] M. Mohammadi, M. Hosseini, M. Shishesaz, A. Hadi, A. Rastgoo, Primary and secondary resonance analysis of porous functionally graded nanobeam resting on a nonlinear foundation subjected to mechanical and electrical loads, *European Journal of Mechanics-A/Solids,* Vol. 77, pp. 103793, 2019.

[20] M. Mohammadi, A. Rastgoo, Nonlinear vibration analysis of the viscoelastic composite nanoplate with three directionally imperfect porous FG core, *Structural Engineering and Mechanics, An Int'l Journal,* Vol. 69, No. 2, pp. 131-143, 2019.

[21] A. Farajpour, A. Rastgoo, M. Mohammadi, Vibration, buckling and smart control of microtubules using piezoelectric nanoshells under electric voltage in thermal environment, *Physica B: Condensed Matter,* Vol. 509, pp. 100-114, 2017.

[22] A. Farajpour, M. H. Yazdi, A. Rastgoo, M. Loghmani, M. Mohammadi, Nonlocal nonlinear plate model for large amplitude vibration of magneto-electro-elastic nanoplates, *Composite Structures,* Vol. 140, pp. 323-336, 2016.

[23] A. Farajpour, M. Yazdi, A. Rastgoo, M. Mohammadi, A higher-order nonlocal strain gradient plate model for buckling of orthotropic nanoplates in thermal environment, *Acta Mechanica,* Vol. 227, No. 7, pp. 1849-1867, 2016.

[24] M. Mohammadi, M. Safarabadi, A. Rastgoo, A. Farajpour, Hygro-mechanical vibration analysis of a rotating viscoelastic nanobeam embedded in a visco-Pasternak elastic medium and in a nonlinear thermal environment, *Acta Mechanica,* Vol. 227, No. 8, pp. 2207-2232, 2016.

[25] M. R. Farajpour, A. Rastgoo, A. Farajpour, M. Mohammadi, Vibration of piezoelectric nanofilm-based electromechanical sensors via higher-order non-local strain gradient theory, *Micro & Nano Letters,* Vol. 11, No. 6, pp. 302-307, 2016.

[26] M. Baghani, M. Mohammadi, A. Farajpour, Dynamic and stability analysis of the rotating nanobeam in a nonuniform magnetic field considering the surface energy, *International Journal of Applied Mechanics,* Vol. 8, No. 04, pp. 1650048, 2016.

[27] M. Goodarzi, M. Mohammadi, M. Khooran, F. Saadi, Thermo-mechanical vibration analysis of FG circular and annular nanoplate based on the visco-pasternak foundation, *Journal of Solid Mechanics,* Vol. 8, No. 4, pp. 788-805, 2016.

[28] H. Asemi, S. Asemi, A. Farajpour, M. Mohammadi, Nanoscale mass detection based on vibrating piezoelectric ultrathin films under thermo-electro-mechanical loads, *Physica E: Low-dimensional Systems and Nanostructures,* Vol. 68, pp. 112-122, 2015.

[29] M. Safarabadi, M. Mohammadi, A. Farajpour, M. Goodarzi, Effect of surface energy on the vibration analysis of rotating nanobeam, 2015.

[30] M. Goodarzi, M. Mohammadi, A. Gharib, Techno-Economic Analysis of Solar Energy for Cathodic Protection of Oil and Gas Buried Pipelines in Southwestern of Iran, in *Proceeding of,* https://publications.waset.org/abstracts/33008/techno-economic-analysis-of …, pp.

[31] M. Mohammadi, A. A. Nekounam, M. Amiri, The vibration analysis of the composite natural gas pipelines in the nonlinear thermal and humidity environment, in *Proceeding of,* https://civilica.com/doc/540946/, pp.

[32] M. Goodarzi, M. Mohammadi, M. Rezaee, Technical Feasibility Analysis of PV Water Pumping System in Khuzestan Province-Iran, in *Proceeding of,* https://publications.waset.org/abstracts/18930/technical-feasibility …, pp.

[33] M. Mohammadi, A. Farajpour, A. Moradi, M. Ghayour, Shear buckling of orthotropic rectangular graphene sheet embedded in an elastic medium in thermal environment, *Composites Part B: Engineering,* Vol. 56, pp. 629-637, 2014.

[34] M. Mohammadi, A. Moradi, M. Ghayour, A. Farajpour, Exact solution for thermo-mechanical vibration of orthotropic mono-layer graphene sheet embedded in an elastic medium, *Latin American Journal of Solids and Structures,* Vol. 11, pp. 437-458, 2014.

[35] M. Mohammadi, A. Farajpour, M. Goodarzi, F. Dinari, Thermo-mechanical vibration analysis of annular and circular graphene sheet embedded in an elastic medium, *Latin American Journal of Solids and Structures,* Vol. 11, pp. 659-682, 2014.

[36] M. Mohammadi, A. Farajpour, M. Goodarzi, Numerical study of the effect of shear in-plane load on the vibration analysis of graphene sheet embedded in an elastic medium, *Computational Materials Science,* Vol. 82, pp. 510-520, 2014.

[37] A. Farajpour, A. Rastgoo, M. Mohammadi, Surface effects on the mechanical characteristics of microtubule networks in living cells, *Mechanics Research Communications,* Vol. 57, pp. 18-26, 2014.

[38] S. R. Asemi, M. Mohammadi, A. Farajpour, A study on the nonlinear stability of orthotropic single-layered graphene sheet based on nonlocal elasticity theory, *Latin American Journal of Solids and Structures,* Vol. 11, pp. 1541-1546, 2014.

[39] M. Goodarzi, M. Mohammadi, A. Farajpour, M. Khooran, Investigation of the effect of pre-stressed on vibration frequency of rectangular nanoplate based on a visco-Pasternak foundation, 2014.

[40] S. Asemi, A. Farajpour, H. Asemi, M. Mohammadi, Influence of initial stress on the vibration of double-piezoelectric-nanoplate systems with various boundary conditions using DQM, *Physica E: Low-dimensional Systems and Nanostructures,* Vol. 63, pp. 169-179, 2014.

[41] S. Asemi, A. Farajpour, M. Mohammadi, Nonlinear vibration analysis of piezoelectric nanoelectromechanical resonators based on nonlocal elasticity theory, *Composite Structures,* Vol. 116, pp. 703-712, 2014.

[42] M. Mohammadi, M. Ghayour, A. Farajpour, Free transverse vibration analysis of circular and annular graphene sheets with various boundary conditions using the nonlocal continuum plate model, *Composites Part B: Engineering,* Vol. 45, No. 1, pp. 32-42, 2013.

[43] M. Mohammadi, M. Goodarzi, M. Ghayour, A. Farajpour, Influence of in-plane pre-load on the vibration frequency of circular graphene sheet via nonlocal continuum theory, *Composites Part B: Engineering,* Vol. 51, pp. 121-129, 2013.

[44] M. Mohammadi, A. Farajpour, M. Goodarzi, R. Heydarshenas, Levy type solution for nonlocal thermo-mechanical vibration of orthotropic mono-layer graphene sheet embedded in an elastic medium, *Journal of Solid Mechanics,* Vol. 5, No. 2, pp. 116-132, 2013.

[45] M. Mohammadi, A. Farajpour, M. Goodarzi, H. Mohammadi, Temperature Effect on Vibration Analysis of Annular Graphene Sheet Embedded on Visco-Pasternak Foundati, *Journal of Solid Mechanics,* Vol. 5, No. 3, pp. 305-323, 2013.

[46] M. Danesh, A. Farajpour, M. Mohammadi, Axial vibration analysis of a tapered nanorod based on nonlocal elasticity theory and differential quadrature method, *Mechanics Research Communications,* Vol. 39, No. 1, pp. 23-27, 2012.

[47] A. Farajpour, A. Shahidi, M. Mohammadi, M. Mahzoon, Buckling of orthotropic micro/nanoscale plates under linearly varying in-plane load via nonlocal continuum mechanics, *Composite Structures*, Vol. 94, No. 5, pp. 1605-1615, 2012.

[48] M. Mohammadi, M. Goodarzi, M. Ghayour, S. Alivand, Small scale effect on the vibration of orthotropic plates embedded in an elastic medium and under biaxial in-plane pre-load via nonlocal elasticity theory, 2012.

[49] A. Farajpour, M. Mohammadi, A. Shahidi, M. Mahzoon, Axisymmetric buckling of the circular graphene sheets with the nonlocal continuum plate model, *Physica E: Low-dimensional Systems and Nanostructures*, Vol. 43, No. 10, pp. 1820-1825, 2011.

[50] A. Farajpour, M. Danesh, M. Mohammadi, Buckling analysis of variable thickness nanoplates using nonlocal continuum mechanics, *Physica E: Low-dimensional Systems and Nanostructures*, Vol. 44, No. 3, pp. 719-727, 2011.

[51] H. Moosavi, M. Mohammadi, A. Farajpour, S. Shahidi, Vibration analysis of nanorings using nonlocal continuum mechanics and shear deformable ring theory, *Physica E: Low-dimensional Systems and Nanostructures*, Vol. 44, No. 1, pp. 135-140, 2011.

[52] M. Mohammadi, M. Ghayour, A. Farajpour, Analysis of free vibration sector plate based on elastic medium by using new version differential quadrature method, *Journal of solid mechanics in engineering*, Vol. 3, No. 2, pp. 47-56, 2011.

[53] A. Farajpour, M. Mohammadi, M. Ghayour, Shear buckling of rectangular nanoplates embedded in elastic medium based on nonlocal elasticity theory, in *Proceeding of*, www.civilica.com/Paper-ISME19-ISME19_390.html, pp. 390.

[54] M. Mohammadi, A. Farajpour, A. R. Shahidi, Higher order shear deformation theory for the buckling of orthotropic rectangular nanoplates using nonlocal elasticity, in *Proceeding of*, www.civilica.com/Paper-ISME19-ISME19_391.html, pp. 391.

[55] M. Mohammadi, A. Farajpour, A. R. Shahidi, Effects of boundary conditions on the buckling of single-layered graphene sheets based on nonlocal elasticity, in *Proceeding of*, www.civilica.com/Paper-ISME19-ISME19_382.html, pp. 382.

[56] M. Mohammadi, M. Ghayour, A. Farajpour, Using of new version integral differential method to analysis of free vibration orthotropic sector plate based on elastic medium, in *Proceeding of*, www.civilica.com/Paper-ISME19-ISME19_497.html, pp. 497.

[57] N. Ghayour, A. Sedaghat, M. Mohammadi, Wave propagation approach to fluid filled submerged visco-elastic finite cylindrical shells, 2011.

[58] M. Mohammadi, A. Farajpour, A. Rastgoo, Coriolis effects on the thermo-mechanical vibration analysis of the rotating multilayer piezoelectric nanobeam, *Acta Mechanica*, https://doi.org/10.1007/s00707-022-03430-0, 2023.

[59] S. E. Ghasemi, A. Ranjbar, M. Hosseini, Numerical study on effect of CuO-water nanofluid on cooling performance of two different cross-sectional heat sinks, *Advanced Powder Technology*, Vol. 28, No. 6, pp. 1495-1504, 2017.

[60] J.-H. Seo, K. S. Garud, M.-Y. Lee, Grey relational based Taguchi analysis on thermal and electrical performances of thermoelectric generator system with inclined fins hot heat exchanger, *Applied Thermal Engineering*, Vol. 184, pp. 116279, 2021.

[61] S. V. Patankar, 2018, *Numerical heat transfer and fluid flow*, CRC press,

[62] A. F. ANSYS, version 14.0: user manual. ANSYS, *Inc., Canonsburg, USA*, 2011.

[63] H. Nabi, M. Pourfallah, M. Gholinia, O. Jahanian, Increasing heat transfer in flat plate solar collectors using various forms of turbulence-inducing elements and CNTs-CuO hybrid nanofluids, *Case Studies in Thermal Engineering*, Vol. 33, pp. 101909, 2022.

[64] B. Kristiawan, A. I. Rifa'i, K. Enoki, A. T. Wijayanta, T. Miyazaki, Enhancing the thermal performance of TiO2/water nanofluids flowing in a helical microfin tube, *Powder Technology*, Vol. 376, pp. 254-262, 2020.